First-principles study of native point defects in hafnia and zirconia

J. X. Zheng,[1] G. Ceder,[1,2] T. Maxisch,[2] W. K. Chim,[1,3] and W. K. Choi[1,3]
[1]*Singapore-MIT Alliance, 4 Engineering Drive 3, Singapore 117576*
[2]*Department of Materials Science and Engineering, Massachusetts Institute of Technology, 77 Massachusetts Avenue, Cambridge, Massachusetts 02139-66307, USA*
[3]*Department of Electrical & Computer Engineering, National University of Singapore, 4 Engineering Drive 3, Singapore 117576*
(Received 16 May 2006; revised manuscript received 27 December 2006; published 14 March 2007)

A first-principles study of native point defects in hafnia (HfO_2) and zirconia (ZrO_2) is carried out to identify dominant defects under different oxygen chemical potentials and Fermi levels. Oxygen vacancies and oxygen interstitials in both HfO_2 and ZrO_2 show negative-U behavior. It is shown that HfO_2 is less prone to the formation of oxygen point defects than ZrO_2 under the same oxygen chemical potential. When the Fermi level is constrained to be within the band gap of silicon, the dominant defects are negatively charged hafnium or zirconium vacancies under intermediate to high oxygen chemical potential. We find no evidence for magnetic defects.

DOI: 10.1103/PhysRevB.75.104112 PACS number(s): 77.84.−s, 74.62.Dh, 71.20.Ps

I. INTRODUCTION

Hafnia (HfO_2) and zirconia (ZrO_2) are two important wide band-gap transition-metal oxide materials. Hafnium (Hf) and zirconium (Zr) have very similar atomic and ionic radii (1.44 and 1.45 Å for Hf and Zr; 0.85 and 0.86 Å for Hf^{4+} and Zr^{4+}) due to the lanthanide contraction in hafnium.[1] The electronegativity value is 1.23 for hafnium and 1.22 for zirconium. Both HfO_2 and ZrO_2 have three polymorphs at atmospheric pressure: the low-temperature phase is monoclinic, and is transformed to a tetragonal phase, and finally to a cubic phase as temperature increases. However, significant differences exist in the transformation temperatures of both materials.[2] The transformation temperature from the monoclinic to the tetragonal phase is about 500 K higher for HfO_2 than for ZrO_2, and that from the tetragonal to the cubic phase is about 200 K higher for HfO_2 than for ZrO_2.

HfO_2 and ZrO_2 are the two more promising candidates to replace silicon dioxide (SiO_2) as the gate dielectric material in metal-oxide-semiconductor (MOS) transistors as the physical thickness of the SiO_2 gate oxide is fast reaching its scaling limit for complementary MOS (CMOS) technologies.[3–16] Both HfO_2 and ZrO_2 have high dielectric constants, relatively high band offsets with respect to silicon, and exhibit good thermodynamic stability in contact with silicon. In particular, HfO_2-based oxides have emerged as the most promising high dielectric constant (high-k) gate dielectric material as they have better thermal stability than ZrO_2.[10–16] However, a few fundamental issues, such as fixed and trapped charges in the material, and the channel mobility reduction they cause, need to be understood and resolved before these high-k dielectrics can be integrated into the conventional silicon CMOS technology.[17–20]

Several theoretical studies on the defect formation energies and energy levels in HfO_2 and ZrO_2 have been carried out: Foster *et al.* studied various defect formation energies and their energy levels in HfO_2 and ZrO_2.[21,22] However, their studies did not consider the chemical potential and Fermi level as controlling variables for defect formation energies. Robertson *et al.* also studied oxygen vacancies and oxygen interstitials in both HfO_2 and ZrO_2, and identified that oxygen vacancies are the main electron traps in both materials.[23,24] Shen *et al.* reported a negative-U behavior for oxygen vacancies in HfO_2.[25] Kang *et al.* suggested that a complex formed by an oxygen vacancy and a hydrogen interstitial (V_O-H) in HfO_2 is responsible for the formation of positive fixed charges after annealing.[26] In this paper we present a comprehensive study of the native point defects in HfO_2 and ZrO_2 as a function of the external chemical potentials and Fermi level as these are the variables that can be controlled by doping and processing conditions.

II. COMPUTATIONAL METHODOLOGY

Our calculations are based on density functional theory (DFT) in the generalized gradient approximation (GGA) with the functional of Perdew, Burke, and Ernzerhof (PBE),[27] for the exchange correlation potential, as implemented in the VASP program (Vienna *ab initio* simulation package).[28] Projector augmented wave (PAW) methods[29,30] are used. The valence electrons for hafnium are generated in the $5p^6 5d^2 6s^2$ configuration and those for zirconium are in the $4s^2 4p^6 4d^2 5s^2$ configuration. The configuration $2s^2 2p^4$ is used for the generation of the valence electrons of oxygen.

In this study, we consider the monoclinic structure for HfO_2 and ZrO_2. This is the low-temperature phase for both HfO_2 and ZrO_2, and is typically present in the gate dielectric film.[4,13,14] In the monoclinic structure, there are two different oxygen sites: O3 is threefold coordinated and O4 is fourfold coordinated by Hf or Zr. Metal ions are surrounded by seven oxygen atoms. Bulk calculations of defect-free HfO_2 and ZrO_2 are performed using a unit cell with 12 atoms. Defect calculations are performed in a $2\times2\times2$ supercell with 96 atoms.

The formalism describing the formation energy of point defects is well established.[31–38] The formation energy of a point defect depends on the chemical potentials as well as on the Fermi level if the point defect is charged. The largest possible range of elemental chemical potentials is given by the stability limit of MO_2 (M=Hf,Zr) with respect to the

 ©2007 The American Physical Society

TABLE I. The monoclinic structural parameters for HfO_2 and ZrO_2.

Reference		a	b	c	β
HfO_2					
44	expt.	5.117	5.175	5.292	99.22
22	GGA	5.132	5.188	5.306	99.78
Present work	GGA	5.137	5.197	5.324	99.39
ZrO_2					
44	expt.	5.151	5.203	5.316	99.20
21	GGA	5.192	5.265	5.358	99.81
Present work	GGA	5.219	5.271	5.411	99.40

pure metal and molecular oxygen. In particular, the ranges of chemical potentials for M (M=Hf,Zr) and O for which the defect energies should be evaluated are

$$\mu_M^o + \Delta E_f^{MO_2} < \mu_M^{MO_2} < \mu_M^o, \tag{1}$$

$$\mu_O^o + \frac{1}{2}\Delta E_f^{MO_2} < \mu_O^{MO_2} < \mu_O^o, \tag{2}$$

where $\mu_M^{MO_2}$ and $\mu_O^{MO_2}$ are chemical potentials for M and O in MO_2, respectively, μ_M^o is the chemical potential of M in the pure metal, μ_O^o is the energy of an oxygen atom in O_2 gas, and $\Delta E_f^{MO_2}$ is the formation enthalpy of MO_2. It should be pointed out that in particular on the reducing side this range of chemical potentials may be too large as sub-valent oxides may form in between the MO_2 compound and the metal which would increase the lowest possible oxygen chemical potential that can be reached. In addition, in GGA the energy of the O_2 molecule is too high compared to the O^{2-} state in the oxide indicating that the maximum oxygen chemical potential on the oxidizing side is probably somewhat too high as well (see Ref. 46).

The formation energy (E_f) of forming a point defect α with charge q, $[\alpha^q]$, in MO_2 (M=Hf,Zr) is computed as

$$E_f[\alpha^q] = E[\alpha^q] \pm \mu_X - E[\text{bulk}] + q(E_V + \Delta V + \varepsilon_F), \tag{3}$$

where $E[\alpha^q]$ is the total energy of the supercell containing the point defect, μ_X is the elemental chemical potential with a positive sign for vacancies and a negative sign for interstitial defects, E [bulk] is the total energy of the perfect supercell, E_V is the valence-band maximum (VBM) of the perfect supercell, and ε_F is the Fermi level which is referenced to E_V. The shift of the VBM in a defect supercell ΔV takes the change of the valence-band maximum caused by the defect into account. It can be obtained using a macroscopic averaging technique[39,40] by calculating the difference between the average electrostatic potential in a bulklike environment of the defect supercell and the average electrostatic potential in the defect-free supercell.

The finite supercell size may contribute interaction between charged defects and their image charges. There is an ongoing debate on whether appropriate *a posteriori* corrections can be applied to the formation energy in order to remove the image charge interactions.[37,41–43] The Makov-Payne correction is a widely used first-order correction to multipole interactions between the image charges and the leading term scales as $1/L$ where L is the size of the supercell. Although the Makov-Payne correction works well for atomic or molecular systems, it overestimates the correction for image charge interactions in solids as it is based on the assumption of localized defect charges and neglects screening from valence electrons. In this study we will show the basic formation energies with and without Makov-Payne corrections, and find that while it changes the values of the formation energies, no significant effect on the nature of the stable defects with oxygen chemical potential or Fermi level is observed.

The thermodynamic transition between two charge states, q_1 and q_2, on the defect occurs for the Fermi level at which the formation energy of $[q_1]$ is equal to that of $[q_2]$. The thermodynamic transition level q_1/q_2 is

$$\varepsilon_F[q_1/q_2] = \frac{1}{q_2 - q_1}\{E[q_1] - E[q_2] + q_1(E_V + \Delta V_1) - q_2(E_V + \Delta V_2)\}, \tag{4}$$

where q_1 and q_2 are the respective initial and final charge states (including the signs), ΔV_1 and ΔV_2 are the VBM shift for the initial and final charge states, respectively, and $\varepsilon_F[q_1/q_2]$ is the Fermi energy level at which the transition from q_1 to q_2 takes place.

III. RESULTS

A. Defect-free bulk HfO_2 and ZrO_2

To converge the total energy of defect-free monoclinic HfO_2 and ZrO_2 to within 10 meV per unit cell, a 500-eV cutoff energy was used for the plane-wave basis and a Monkhorst-Pack $6 \times 6 \times 6$ k-point grid for the Brillouin-zone integration. The calculated monoclinic structural parameters, shown in Table I, are close to experimental data, but show the rather consistent overestimation common for GGA.

Although the problem of calculating the O_2 binding energy in DFT is well documented,[45,46] and results in inaccuracy in calculating the enthalpy of formation from O_2 gas we show the calculated enthalpy of formation for HfO_2 and ZrO_2 in Table II as they define the range for the elemental chemical potential used in the subsequent defect energy cal-

TABLE II. The calculated and experimental enthalpy of formation for HfO_2 and ZrO_2.

	Calculated (eV/formula unit)	Experimental (eV/formula unit)
HfO_2	−11.278	−11.864
ZrO_2	−10.662	−11.407

culations. The experimental values from Ref. 47 are also included.

The total electron density of states (DOS), as well as their atomic and orbital projected DOS, for HfO_2 and ZrO_2 are shown in Fig. 1. For both materials, the top of the valence band is dominated by O $2p$ states while the bottom of the conduction band is dominated by metal (Hf, Zr) d states. The calculated band gap for HfO_2 is 3.9 eV, which is smaller than the experimental value[48] of 5.9 eV. ZrO_2 has a calculated band gap of 3.4 eV, which is smaller than the experimental value[49,50] of 5.4 eV. The underestimation of the band-gap energy value is typical of DFT calculations in the GGA approximation.

B. Defect formation energies

The calculation of defects requires a larger supercell than for defect-free bulk compounds and allows therefore a reduced k-point grid. We found that for a supercell containing 96 atoms the formation energies of point defects obtained with a $2\times2\times2$ or $4\times4\times4$ Monkhorst-Pack k-point grid differ by less than 10 meV. Hence a $2\times2\times2$ Monkhorst-Pack k-point grid is used for defect calculations in our study.

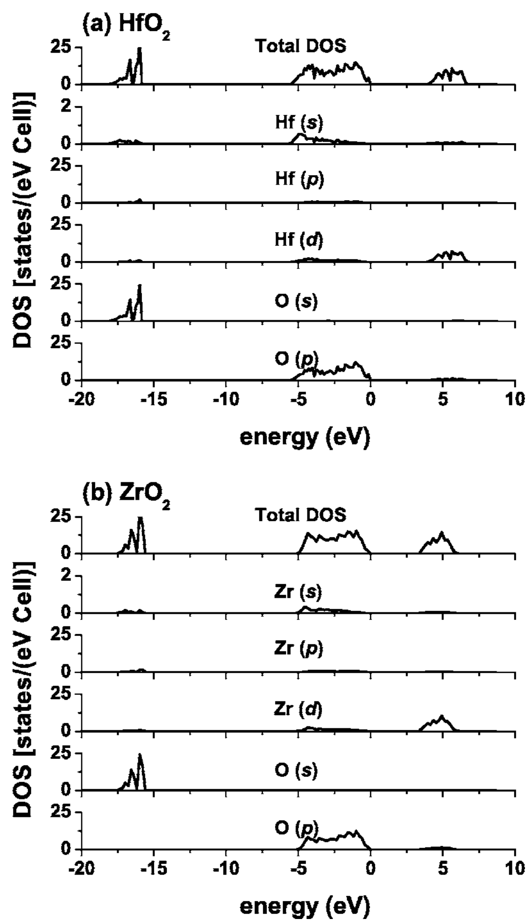

FIG. 1. Total DOS and orbital projected DOS for (a) HfO_2 and (b) ZrO_2.

We have calculated the formation energies for native point defects in HfO_2 and ZrO_2, including oxygen vacancy (V_O), metal vacancy (V_M), oxygen interstitial (O_i), metal interstitial (M_i), oxygen antisite (O_M), and metal antisite (M_O). The stable neutral oxygen interstitial forms a dumbbell-shaped defect pair with a threefold-coordinated oxygen atom, which is the same as that described by Foster and co-workers.[21,22] The metal interstitials are most stable at $2c$ sites [at position (0 1/4 0) in a monoclinic unit cell], which are octahedrally coordinated by six oxygen atoms.

The formation energy of point defects in various charge states at the VBM ($\varepsilon_F=0$ eV) under extreme oxidation condition ($\mu_O=\mu_O^o$) and extreme reducing condition ($\mu_M=\mu_M^o$) are given in Table III without image charge corrections.

It is useful to compare the energy difference for oxygen point defects in HfO_2 and ZrO_2 with the work of Foster *et al.*,[21,22] even though different pseudopotentials were used. It is noted that no image charge corrections were applied to the defect formation energies in Foster *et al.*'s work. The energy differences for V_{O3} and V_{O4} between HfO_2 and ZrO_2 are 0.50 and 0.48 eV, respectively, which are close to the values of 0.48 and 0.46 eV obtained by Foster *et al.* For O_i, the energy difference is 0.27 eV, comparable to 0.2 eV shown by Foster *et al.*

The formation energies for different defects in ZrO_2 and HfO_2 are shown in Fig. 2 as a function of Fermi level for the two limiting values of the oxygen chemical potentials and for one intermediate oxygen chemical potential. The lower limit for the Fermi level ($\varepsilon_F=0$ eV) corresponds to the top of the valence band while the upper limit ($\varepsilon_F=E_g$) represents the bottom of the *experimental* conduction band. The energy of a defect with a particular charge state is only shown for the range of Fermi levels where that charge state has the lowest energy. Hence the slope of the lines in these figures corresponds to the charge state of the defect and changes in slope indicate a transition between charge states. In Fig. 2, the defect formation energies are corrected for image charge interactions. Thereby, we use the leading term (L^{-1} term) in the Makov-Payne correction scheme as an upper bound estimation for the image charge correction. The L^{-1} term scales proportionally with q^2, where q is the total cell charge. For ±4 charge defects the upper bound of the image charge interaction is estimated to be 1.57 eV for HfO_2 and 1.55 eV for ZrO_2 when the dielectric constant $\varepsilon=20$ is used.[8,51,52] The image charge corrections for different charge states in HfO_2 and ZrO_2 are shown in Table IV.

The VBM of the silicon, E_V(Si), are shown as vertical dashed lines. The position of E_V(Si) with respect to the VBM of MO_2 is determined by alignment of the macroscopic average of the electrostatic potential across the Si/oxide interface. Previous computational studies on the band offsets of HfO_2 and ZrO_2 on Si have shown that the calculated valence-band offsets for oxygen terminated interfaces correspond well to the experimental values.[53,54] The valence-band

TABLE III. Point defect formation energies (E_f) without image charge corrections in HfO_2 and ZrO_2 at $\mu_M=\mu_M^o$ (M=Hf,Zr) and $\mu_O=\mu_O^o$ at VBM ($\varepsilon_F=0$ eV).

Defect	Charge on defect	Kröger-Vink notation	E_f in HfO_2 (eV)		E_f in ZrO_2 (eV)	
			$\mu_M=\mu_M^o$	$\mu_O=\mu_O^o$	$\mu_M=\mu_M^o$	$\mu_O=\mu_O^o$
V_{O3}	0	V_{O3}^X	1.12	6.76	0.93	6.26
V_{O3}	+1	$V_{O3}^{\bullet}$	−1.66	3.98	−1.79	3.54
V_{O3}	+2	$V_{O3}^{\bullet\bullet}$	−4.83	0.81	−4.79	0.54
V_{O4}	0	V_{O4}^X	0.98	6.63	0.82	6.15
V_{O4}	+1	$V_{O4}^{\bullet}$	−1.39	4.25	−1.45	3.88
V_{O4}	+2	$V_{O4}^{\bullet\bullet}$	−4.20	1.44	−4.10	1.23
V_M	0	V_M^X	17.01	5.73	16.44	5.78
V_M	−1	V_M'	16.97	5.69	16.38	5.72
V_M	−2	V_M''	16.99	5.71	16.37	5.71
V_M	−3	V_M'''	17.07	5.79	16.42	5.76
V_M	−4	V_M''''	17.26	5.98	16.53	5.87
O_i	0	O_i^X	7.22	1.58	6.64	1.31
O_i	−1	O_i'	9.04	3.40	8.52	3.19
O_i	−2	O_i''	9.52	3.88	8.90	3.57
M_i	0	M_i^X	5.35	16.63	3.61	14.28
M_i	+1	$M_i^{\bullet}$	2.05	13.33	0.71	11.38
M_i	+2	$M_i^{\bullet\bullet}$	−1.54	9.74	−2.40	8.26
M_i	+3	$M_i^{\bullet\bullet\bullet}$	−4.26	7.02	−4.67	5.99
M_i	+4	$M_i^{\bullet\bullet\bullet\bullet}$	−7.13	4.15	−7.08	3.58
M_O	0	M_O^X	5.29	22.21	6.95	22.94
M_O	+1	$M_O^{\bullet}$	1.85	18.77	3.72	19.71
M_O	+2	$M_O^{\bullet\bullet}$	−1.77	15.16	0.26	16.26
M_O	+3	$M_O^{\bullet\bullet\bullet}$	−4.67	12.25	−3.30	12.69
M_O	+4	$M_O^{\bullet\bullet\bullet\bullet}$	−7.55	9.37	−5.95	10.05
O_M	0	O_M^X	20.85	3.93	19.74	3.75
O_M	−1	O_M'	20.92	4.00	19.77	3.78
O_M	−2	O_M''	21.16	4.24	20.09	4.10

offset we used in this study is 3.15 eV for ZrO_2,[55,56] and 3.4 eV for HfO_2.[57] The silicon conduction-band minimum, E_C(Si), is not drawn in the figure as its position is uncertain within the DFT framework.

IV. DISCUSSION

For ZrO_2 under low oxygen partial pressure (and high zirconium partial pressure), all stable defects create oxygen deficiency. Zr_i is the dominant defect when the Fermi level is close to the VBM of ZrO_2 [see Fig. 2(a)] while V_O becomes dominant as the Fermi level increases. Increasing the oxygen partial pressure reduces the stability of the zirconium interstitial so that it cannot be stabilized even for a low Fermi level [Fig. 2(b)]. Instead, V_O is stable at low Fermi level. At higher Fermi level, the formation of zirconium vacancies is favorable. Under the highest oxygen partial pressure [Fig. 2(c)], V_O and O_i dominate over a narrow range when the Fermi level is close to the VBM and V_{Zr} dominates when the Fermi level is further away from the VBM. Generally, the formation of native point defects in HfO_2 is similar except that the hafnium antisite (Hf_O) can form when the Fermi level is close to the VBM and the oxygen partial pressure is very low [Fig. 2(a), right panel]. This can be understood because the minimum value of μ_O possible in the oxide [for which Fig. 2(a) is plotted] is lower value in HfO_2 than in ZrO_2 due to the more negative formation enthalpy of HfO_2. Though image charge corrections were applied to obtain Fig. 2, we find that the variation of defect type with Fermi level and oxygen chemical potential does not qualitatively change without the corrections, even though the absolute values of the defect formation energies are modified.

Oxygen interstitials in HfO_2 and ZrO_2 exhibit a "negative-U" behavior, i.e., O_i^- is not stable against O_i and O_i^{-2}. As an oxygen interstitial adds three $2p$ states and four $2p$ electrons to the top of the valence band, the defect levels

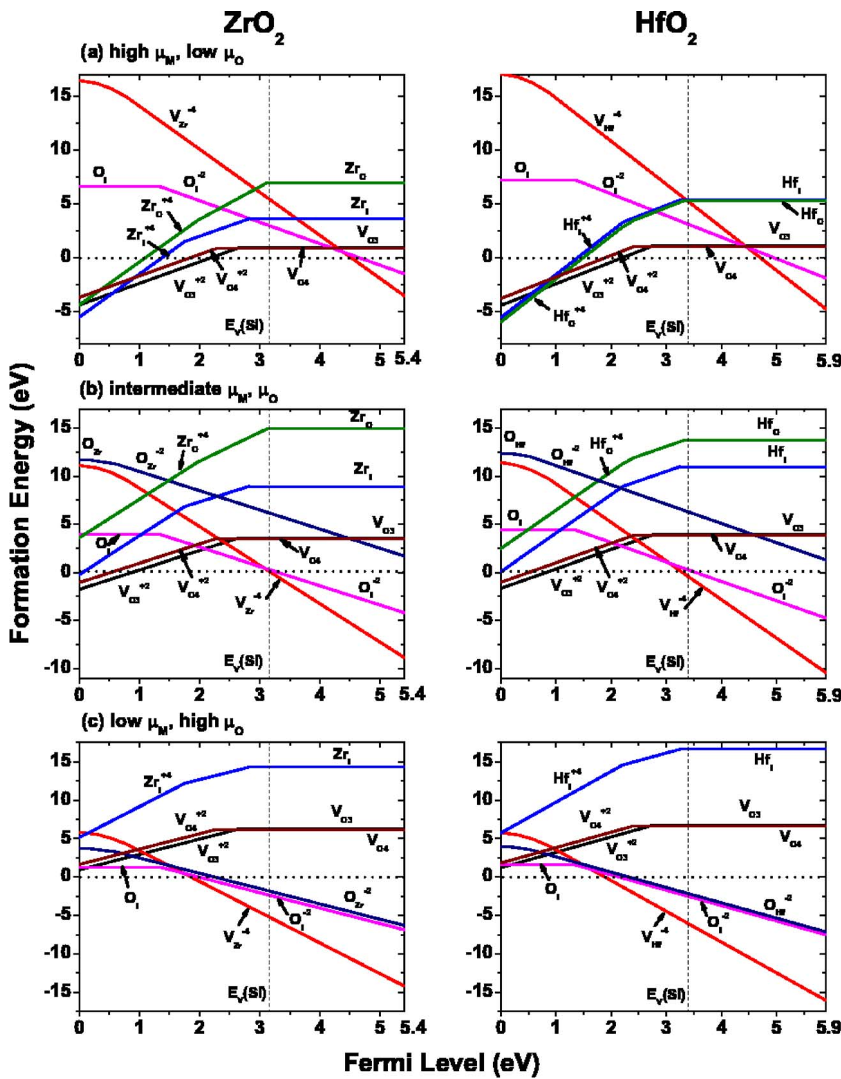

FIG. 2. (Color online) Calculated defect formation energy for native point defects in ZrO_2 and HfO_2 as a function of Fermi level and for (a) $\mu_O = \mu_O^o + \frac{1}{2}\Delta E_f^{MO_2}$ (low oxygen partial pressure and high metal partial pressure), (b) $\mu_O = \mu_O^o + \frac{1}{4}\Delta E_f^{MO_2}$ (intermediate oxygen and metal partial pressure), and (c) $\mu_O = \mu_O^o$ (high oxygen partial pressure and low metal partial pressure). The image charge corrections have been applied. The positions of the valence-band maximum of the silicon $[E_V(\text{Si})]$ are marked by vertical dashed lines.

caused by oxygen interstitials exhibit valence-band character and the formation energy for oxygen interstitials is unlikely to be significantly affected by the underestimation of the band gap. The negative-*U* behavior for oxygen interstitials is in agreement with studies by Foster and co-workers.[21,22]

Oxygen vacancies in HfO_2 and ZrO_2 also show "negative-*U*" behavior, i.e., V_o^+ is not stable against disproportionation into V_o and V_o^{+2}. Similar to the oxygen vacancy levels in Y_2O_3,[38] the defect levels from oxygen vacancies in HfO_2 and ZrO_2 have conduction-band (CB) character. Hence corrections to the band gap which would move the CB towards higher energies are likely to increase the formation energy of oxygen vacancies with filled electron levels as these may move up with the conduction band. Under this scenario, the formation energy for V_o would increase at twice the rate of the energy for V_o^+ as there are two electrons occupying the defect level for V_o and one electron for V_o^+. The formation energy for V_o^{+2} is not affected by any band-gap correction. Thus the thermodynamic transition energy levels, i.e., $(0/+)$, $(+/+2)$, and $(0/+2)$, for oxygen vacancies would be shifted upward by a similar amount as a band-gap error correction is applied. Therefore our conclusion on negative *U* for oxygen vacancies is likely to be independent of DFT band-gap errors. Recent studies[24,25] also showed negative *U* for oxygen vacancies, and Shen *et al.* argued that it can explain the frequency dependence of charge trapping. The thermodynamic transition energy level $(0/+2)$ is located at 1.12 eV for the O3 vacancy, and at 1.50 eV for the O4 vacancy below the calculated CBM of HfO_2. In ZrO_2, the level $(0/+2)$ is located at 0.74 eV for the O3 vacancy and 1.13 eV for the O4 vacancy below the calculated CBM. Note that the calculated CBM is located at $\varepsilon_F = 3.9$ eV for HfO_2 and $\varepsilon_F = 3.4$ eV for ZrO_2. As the band-gap underestimations are similar for both materials, the locations of defect levels from

TABLE IV. The image charge corrections for different charge states in HfO_2 and ZrO_2.

Charge state	HfO_2 (eV)	ZrO_2 (eV)
±1	0.10	0.10
±2	0.39	0.38
±3	0.88	0.87
±4	1.57	1.55

oxygen vacancies lie deeper below the experimental CBM in HfO_2 than in ZrO_2.

At high oxygen partial pressure $(\mu_O=\mu_O^o)$ oxygen defects have higher energy in HfO_2 than in ZrO_2 (Table III). The formation energy of oxygen vacancies is more than 200 meV higher in HfO_2 than in ZrO_2 and the formation energy of oxygen interstitials is about 200 meV higher in HfO_2 than in ZrO_2. This suggests that HfO_2 is less prone to the formation of oxygen point defects than ZrO_2 under the same oxygen chemical potential condition.

Recent reports[58,59] have observed unexpected ferromagnetism in HfO_2 thin films. A first-principles study by Pemmaraju and Sanvito suggests that hafnium vacancies are a possible origin for the ferromagnetism.[60] Later experiments, however, have shown that the ferromagnetism in HfO_2 is introduced by contaminations through handling with stainless-steel tweezers.[61] In principle, defects with unpaired electrons could carry a magnetic moment. In our study, we do not find any stable defects that carry a magnetic moment and the neutral hafnium vacancies are unlikely to form since their formation energies are high. Hence native point defects are unlikely to cause ferromagnetism in HfO_2.

When either HfO_2 or ZrO_2 is used as a gate insulator material in MOS devices, the electron reservoir to form a charged defect is provided by the polysilicon gate or the silicon substrate. This limits the range for the electron chemical potential to be between the valence-band maximum $[E_V(\text{Si})]$ and the conduction-band minimum $[E_C(\text{Si})]$ of Si. Although $E_C(\text{Si})$ is not included in Fig. 2 as its relative position is uncertain within the DFT framework, in the reasonable range of Fermi levels above $E_V(\text{Si})$ charged zirconium or hafnium vacancies are dominant. Only under very low oxygen chemical potential [Fig. 2(a)] does the V_O appear. As normal deposition conditions for gate dielectrics correspond to a regime somewhere between intermediate and high oxygen partial pressure, the negatively charged zirconium or hafnium vacancies are expected to be the dominant defects. They are likely to cause negative fixed charges near the Si/oxide interfacial region, as has been observed experimentally after deposition of gate oxide films.[9,16] After post-deposition annealing, positive oxide fixed charges are observed. Kang *et al.* suggested that the V_O-H complex is responsible for the formation of positive oxide fixed charges.[26]

It needs to be noted that many of the defect formation energies in Fig. 2 are negative. Some of the negative values at the extremes of oxygen chemical potential may reflect the fact that these chemical potentials are not really achievable. At the low end of oxygen chemical potential it is possible that suboxides would form before reduction to the metal takes place which would restrict the lower value of oxygen potential that can be achieved in ZrO_2 and HfO_2. On the high oxidation side the underestimation of the binding energy of O_2 (Ref. 46) allows for too high an oxygen chemical potential in our model leading to a substantial trend to form metal vacancies. But the negative formation energies at intermediate chemical potentials of oxygen cannot be attributed to these issues and may reflect a real instability in the material at some values of the Fermi level. In semiconductors, such negative formation energies would lead to Fermi-level pinning as defects would spontaneously form and generate valence-band or conduction-band carriers until the change in the Fermi level makes the defect energy positive. This concept is unlikely to be applicable to insulating oxides such as HfO_2 and ZrO_2 where carriers are localized and do not exhibit a bandlike character. Except at interfaces, where the material can deviate from local neutrality, charged defects in these oxides can only form in the bulk when other defects of opposite charge are also present. However, such combinations of positively and negatively charged defects never seem to have negative formation energies for the intermediate values of the Fermi level in Fig. 2. The negative formation energies may however have implications for the presence of charges at the Si/oxide interface where a true Fermi-level reservoir of charges is available from the Si.

V. CONCLUSIONS

A first-principles study of point defects in HfO_2 and ZrO_2 has been performed. Dominant defects in both materials show similar behavior. Metal interstitials, oxygen vacancies and interstitials, and metal vacancies can occur depending on the external chemical potentials and Fermi level. However in HfO_2 we find that under high hafnium chemical potential, hafnium antisite is possible. In both HfO_2 and ZrO_2, oxygen interstitials and oxygen vacancies show negative-U behavior. HfO_2 is less prone to the formation of oxygen point defects than ZrO_2. When the Fermi level is constrained to the band gap of silicon, negatively charged metal vacancies are dominant defects except for very low oxygen chemical potential under which oxygen vacancies may occur.

ACKNOWLEDGMENTS

The authors would like to thank the Singapore-MIT Alliance (SMA) and the National University of Singapore (NUS) for supporting this work. T. M. acknowledges the support by the Department of Energy under Contract No. DE-FG02-96ER45571 and by the MRSEC program of the National Science Foundation under Contract No. DMR-0213282. Additional computing resources were provided by the National Science Foundation, National Partnership for Advanced Computing Infrastructure (NPACI). J.X. Zheng acknowledges financial support from SMA and NUS.

[1] F. A. Cotton, G. Wilkinson, C. A. Murillo, and M. Bochmann, *Advanced Inorganic Chemistry*, 6th ed. (John Wiley, & Sons, New York, 1999).
[2] I. Barin, *Thermochemical Data of Pure substances*, 3rd ed. (VCH, Weinheim, 1995).
[3] M. Houssa, *High-k Gate Dielectrics* (Institute of Physics, Bristol and Philadelphia, 2004).
[4] M. Copel, M. Gribelyuk, and E. Gusev, Appl. Phys. Lett. **76**, 436 (2000).
[5] T. S. Jeon, J. M. White, and D. L. Kwong, Appl. Phys. Lett. **78**, 368 (2001).
[6] W. J. Qi, R. Nieh, B. H. Lee, L. Kang, Y. J. Joen, and J. C. Lee, Appl. Phys. Lett. **77**, 3269 (2000).
[7] E. P. Gusev, E. Cartier, D. A. Buchanan, M. Gribelyuk, M. Copel, H. Okorn-Schmidt, and C. D'Emic, Microelectron. Eng. **59**, 341 (2001).
[8] G. D. Wilk, R. M. Wallace, and J. M. Anthony, J. Appl. Phys. **89**, 5243 (2001).
[9] M. Houssa, V. V. Afanas'ev, A. Stesmans, and M. M. Heyns, Appl. Phys. Lett. **77**, 1885 (2000).
[10] B. H. Lee, L. Kang, R. Nieh, W. J. Qi, and J. C. Lee, Appl. Phys. Lett. **76**, 1926 (2000).
[11] E. P. Gusev, C. Cabral, Jr., M. Copel, C. D'Emic, and M. Gribelyuk, Microelectron. Eng. **69**, 145 (2003).
[12] S. J. Lee, T. S. Jeon, D. L. Kwong, and R. Clark, J. Appl. Phys. **92**, 2807 (2002).
[13] K. Kukli, M. Ritala, J. Sundqvist, J. Aarik, J. Lu, T. Sajavaara, M. Leskela, and A. Harsta, J. Appl. Phys. **92**, 5698 (2002).
[14] M.-H. Cho, Y. S. Roh, C. N. Whang, K. Jeong, S. W. Nahm, D.-H. Ko, J. H. Lee, N. I. Lee, and K. Fujihara, Appl. Phys. Lett. **81**, 472 (2002).
[15] J. Kim, S. Kim, H. Jeon, M.-H. Cho, K.-B. Chung, and C. Bae, Appl. Phys. Lett. **87**, 053108 (2005).
[16] S. J. Lee, C. H. Choi, A. Kamath, R. Clark, and D. L. Kwong, IEEE Electron Device Lett. **24**, 105 (2003).
[17] A. Kerber, E. Cartier, L. Pantisano, R. Degraeve, T. Kauerauf, Y. Kim, A. Hou, G. Groeseneken, H. E. Maes, and U. Schwalke, IEEE Electron Device Lett. **24**, 87 (2003).
[18] G. D. Wilk and D. A. Muller, Appl. Phys. Lett. **83**, 3984 (2003).
[19] S. Zafar, A. Kumar, E. Gusev, and E. Cartier, IEEE Trans. Device Mater. Reliab. **5**, 45 (2005).
[20] D. Lim and R. Haight, J. Vac. Sci. Technol. B **23**, 201 (2005).
[21] A. S. Foster, V. B. Sulimov, F. L. Gejo, A. L. Shluger, and R. M. Nieminen, Phys. Rev. B **64**, 224108 (2001).
[22] A. S. Foster, F. L. Gejo, A. L. Shluger, and R. M. Nieminen, Phys. Rev. B **65**, 174117 (2002).
[23] J. Robertson, K. Xiong, and B. Falabretti, IEEE Trans. Device Mater. Reliab. **1**, 84 (2005).
[24] K. Xiong, J. Robertson, M. C. Gibson, and S. J. Clark, Appl. Phys. Lett. **87**, 183505 (2005).
[25] C. Shen, M. F. Li, X. P. Wang, H. Y. Yu, Y. P. Feng, A. T.-L. Lim, Y. C. Yeo, D. S. H. Chan, and D. L. Kwong, Tech. Dig. - Int. Electron Devices Meet. **2004**, 733.
[26] J. Kang, E.-C. Lee, K. J. Chang, and Y. G. Jin, Appl. Phys. Lett. **84**, 3894 (2004).
[27] J. P. Perdew, K. Burke, and M. Ernzerhof, Phys. Rev. Lett. **77**, 3865 (1996).
[28] G. Kresse and J. Furthmüller, Phys. Rev. B **54**, 11169 (1996); G. Kresse and J. Furthmüller, Comput. Mater. Sci. **6**, 15 (1996).
[29] G. Kresse and D. Joubert, Phys. Rev. B **59**, 1758 (1999).
[30] P. E. Blöchl, Phys. Rev. B **50**, 17953 (1994).
[31] A. F. Kohan, G. Ceder, D. Morgan, and C. G. Van de Walle, Phys. Rev. B **61**, 15019 (2000).
[32] S. B. Zhang, S.-H. Wei, and A. Zunger, Phys. Rev. B **63**, 075205 (2001).
[33] D. B. Laks, C. G. Van de Walle, G. F. Neumark, P. E. Blöchl, and S. T. Pantelides, Phys. Rev. B **45**, 10965 (1992).
[34] A. Garcia and J. E. Northrup, Phys. Rev. Lett. **74**, 1131 (1995).
[35] S. Pöykkö, M. J. Puska, and R. M. Nieminen, Phys. Rev. B **53**, 3813 (1996).
[36] K. W. Kwak, D. Vanderbilt, and R. D. King-Smith, Phys. Rev. B **52**, 11912 (1995).
[37] C. G. Van de Walle and J. Neugebauer, J. Appl. Phys. **95**, 3851 (2004).
[38] J. X. Zheng, G. Ceder, T. Maxisch, W. K. Chim, and W. K. Choi, Phys. Rev. B **73**, 104101 (2006).
[39] A. Baldereschi, S. Baroni, and R. Resta, Phys. Rev. Lett. **61**, 734 (1988).
[40] M. Peressi, N. Binggeli, and A. Baldereschi, J. Phys. D **31**, 1273 (1998).
[41] G. Makov and M. C. Payne, Phys. Rev. B **51**, 4014 (1995).
[42] C. Persson, Y. J. Zhao, S. Lany, and A. Zunger, Phys. Rev. B **72**, 035211 (2005).
[43] J. Shim, E. K. Lee, Y. J. Lee and R. M. Nieminen, Phys. Rev. B **71**, 035206 (2005).
[44] R. E. Hann, P. R. Suitch, and J. L. Pentecost, J. Am. Ceram. Soc. **68**, 285 (1985).
[45] B. Hammer, L. B. Hansen, and J. K. Nørskov, Phys. Rev. B **59**, 7413 (1999).
[46] L. Wang, T. Maxisch, and G. Ceder, Phys. Rev. B **73**, 195107 (2006).
[47] J. G. Speight, *Lange's Handbook of Chemistry*, 16th ed. (McGraw-Hill, New York, 2005).
[48] V. V. Afanas'ev, A. Stesmans, F. Chen, X. Shi, and S. A. Campbell, Appl. Phys. Lett. **81**, 1053 (2002).
[49] M. Houssa, M. Tuominen, M. Naili, V. Afanas'ev, A. Stesmans, S. Haukka, and M. M. Heynes, J. Appl. Phys. **87**, 8615 (2000).
[50] B. Králik, E. K. Chang, and S. G. Louie, Phys. Rev. B **57**, 7027 (1998).
[51] X. Y. Zhao and D. Vanderbilt, Phys. Rev. B **65**, 075105 (2002).
[52] X. Y. Zhao and D. Vanderbilt, Phys. Rev. B **65**, 233106 (2002).
[53] P. W. Peacock, K. Xiong, K. Tse, and J. Robertson, Phys. Rev. B **73**, 075328 (2006).
[54] Y. F. Dong, Y. P. Feng, S. J. Wang, and A. C. H. Huan, Phys. Rev. B **72**, 045327 (2005).
[55] S. Miyazaki, Appl. Surf. Sci. **190**, 66 (2002).
[56] S. Miyazaki, J. Vac. Sci. Technol. B **19**, 2212 (2001).
[57] S. Sayan, E. Garfunkel, and S. Suzer, Appl. Phys. Lett. **80**, 2135 (2002).
[58] M. Venkatesan, C. B. Fitzgerald, and J. M. D. Coey, Nature (London) **430**, 630 (2004).
[59] J. M. D. Coey, M. Venkatesan, P. Stamenov, C. B. Fitzgerald, and L. S. Dorneles, Phys. Rev. B **72**, 024450 (2005).
[60] C. D. Pemmaraju and S. Sanvito, Phys. Rev. Lett. **94**, 217205 (2005).
[61] D. W. Abraham, M. M. Frank, and S. Guha, Appl. Phys. Lett. **87**, 252502 (2005).